COMPUTATIONAL AEROELASTIC ANALYSES OF A LOW-BOOM SUPERSONIC CONFIGURATION

Walter A. Silva[1], Mark D. Sanetrik[1], Pawel Chwalowski[1], and Joseph Connolly[2]

[1]Aeroelasticity Branch
NASA Langley Research Center
Hampton, Virginia, USA
Walter.A.Silva@nasa.gov

[2]Intelligent Control and Autonomy Branch
NASA Glenn Research Center
Cleveland, Ohio, USA

Keywords: supersonic aeroservoelasticity, computational aeroelasticity, ROM.

Abstract:

An overview of NASA's Commercial Supersonic Technology (CST) Aeroservoelasticity (ASE) element is provided with a focus on recent computational aeroelastic analyses of a low-boom supersonic configuration developed by Lockheed-Martin and referred to as the N+2 configuration. The overview includes details of the computational models developed to date including a linear finite element model (FEM), linear unsteady aerodynamic models, unstructured CFD grids, and CFD-based aeroelastic analyses. In addition, a summary of the work involving the development of aeroelastic reduced-order models (ROMs) and the development of an aero-propulso-servo-elastic (APSE) model is provided.

1 INTRODUCTION

The unique structural configuration of supersonic aircraft combined with nonlinear aerodynamics and rigid-body effects often results in highly complex nonlinear aeroelastic/flight dynamics phenomena. These aeroelastic phenomena can affect ride quality, gust loads, flutter, flight dynamics and control, and engine performance. The aeroelastic/flight dynamics phenomena simultaneously influence the airframe and propulsion system controls, producing undesirable effects on performance and flying characteristics.

These ASE phenomena need to be thoroughly understood in order for supersonic flight to be safe, efficient, and comfortable. In addition, there is an opportunity, through active controls, to exploit these phenomena for improved performance and efficiency. Analysis and design capabilities for slender supersonic aircraft may then be enhanced by including this new knowledge.

A vast body of analytical, computational, wind-tunnel, and flight data exist on the ASE characteristics of subsonic transport and supersonic fighter aircraft [1]. Systems for control of undesirable aeroelastic phenomena, such as suppression of flutter, have been demonstrated in the past [2–5]. Systems that exploit vehicle flexibility for improved performance, such as vehicle roll control beyond aileron reversal and wing load alleviation have also been demonstrated [6, 7].

Considerably less data are available for supersonic cruise configurations. In the mid- to late-1990s, as part of the High Speed Research (HSR) program, research was performed in the areas of computational and experimental aeroelasticity [8]. As part of this research, aeroelastic wind-tunnel models were designed, built, and tested in the Transonic Dynamics Tunnel (TDT). A remnant from the HSR program is the Semi-Span Super-Sonic Transport (S4T) [9], a very sophisticated, aeroelastically-scaled semispan wind-tunnel model based on the Technology Concept Aircraft configuration equipped with three active surfaces (ride control vane, aileron, horizontal tail) and flow-through nacelles with flexible mounts. The model was designed so that it would flutter within the TDT operating boundary, making it an ideal testbed for investigating ASE issues associated with supersonic cruise configurations.

Under the auspices of the Supersonics Program within NASA's Fundamental Aeronautics Program (FAP), the S4T was the subject of four experiments in the TDT: two open-loop (no feedback control) tests and two closed-loop (with feedback control) tests over the span of three years between 2007 and 2010. A special session on the various aspects of the S4T program was organized for the AIAA Structures, Structural Dynamics, and Materials conference held in 2012. The work involving the S4T was completed in 2012.

The Supersonics Program was renamed the High Speed Program and recently renamed again to the Commercial Supersonic Technology (CST) Project. The CST Project, still a component of NASA's FAP, continues the original charter of the Supersonics Program, addressing the technical barriers to safe, efficient, and economical supersonic flight. One of the elements within the CST Project is ASE, tasked with addressing the aeroelastic (AE), ASE, and APSE challenges associated with low-boom supersonic configurations. In order to address more realistic challenges associated with a full-span configuration, including rigid-body modes, the CST ASE element is now focusing on a full-span low-boom configuration.

A top priority for the CST ASE element is to develop the tools required to perform accurate, high fidelity computational AE, ASE, and APSE analyses in support of the design of future low-boom high speed civil aircraft. As a means of accomplishing that priority, the CST project collaborated with Lockheed-Martin to conduct such analyses. Under the NASA N+2 (two generations from present state) contract, Lockheed-Martin developed a low-boom supersonic configuration and a detailed FEM. Artist renderings of two views of the Lockheed-Martin N+2 configuration are presented in Figure 1 and Figure 2. The goal of the N+2 effort is to develop and validate technologies for future civil supersonic airliners. Primary activities under this effort included Low Boom Wind Tunnel Testing, Propulsion System Maturation, Optimization Method Development, Structural and Aeroelastic Analysis, and System Studies.

Figure 1: Artist's concept of the Lockheed-Martin N+2 configuration.

Figure 2: Artist's concept of the Lockheed-Martin N+2 configuration.

In addition to the analysis of the N+2 configuration, the CST ASE element is also involved in the development of APSE models. The development of an APSE model consists of the interconnection of a traditional ASE model (airframe model) with a dynamic engine model. Traditionally, these two models are developed and used separately by distinct disciplines (such as ASE and propulsion performance). The ultimate goal of this development is to be able to determine if the airframes flexibility has an effect on the thrust

dynamics of the propulsion system, coupling back to the airframe flexibility modes as a closed loop system, in order to study performance like vehicle stability and ride quality.

This paper will address results from prior publications [10,11] as well as recent accomplishments. The paper begins with a description of the Lockheed-Martin N+2 configuration followed by a description of the structural sizing and analysis leading to an FEM. Parametric studies that consist of inclusion of metallic components are discussed. Recent and updated linear aeroelastic analyses are presented as well. The vehicle design, sizing, FEM analyses/parametrics, linear aeroelastic analyses, and CFD loads analyses were performed by Lockheed-Martin [10, 11]. Unstructured grids of the N+2 configuration, generated at NASA, are presented along with Euler (inviscid) static aeroelastic and sonic boom propagation results at a cruise condition. Finally, a summary of the work being performed in the area of ROM and APSE model developments is presented.

2 N+2 CONFIGURATION

In this section, general characteristics of the N+2 configuration are presented. Shown in Figure 3 are four different views: a planform view (Figure 3(a)), a side view (Figure 3(b)), an isometric view (Figure 3(c)), and a front view (Figure 3(d)). Of particular interest are the three engines, one mounted aft and on top while the other two are mounted below and close to the fuselage. From an initial and cursory point of view, this arrangement would not seem to pose any obvious aeroelastic issues. In fact, the two engines mounted below offer some relief from possible aeroelastic issues by being installed close to the fuselage instead of further out on the span of the wing. However, having these large masses at the tail of a flexible fuselage is likely to cause some aeroelastic issues.

(a) Planform view.

(b) Side view.

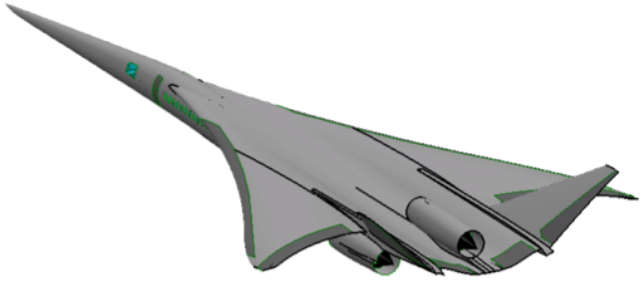

(c) Isometric view.

(d) Front view.

Figure 3: Different views of the N+2 configuration.

Presented in Table 1 are the general characteristics of the vehicle. At a length of 244 ft., the N+2 configuration is about 21% longer than the Concorde but at about the same wingspan. However, the N+2 configuration is lighter than the Concorde, with a cruising Mach number of 1.7 that is lower than that of the Concorde (cruise M=2.02), but with a greater range.

3 STRUCTURAL LAYOUT AND FEM

As a first step towards performing realistic aeroelastic analyses, Lockheed-Martin developed a detailed structural layout of the configuration. Presented in Figure 4 is a sample image of the substructure of the vehicle. The goal of the finite element modeling effort

Table 1: N+2 Configuration

Length	244 ft.
Span	83 ft. 10 in.
Height	(Overall) 30 ft. 6 in. (Doorsill) 7 ft. 7 in.
Weight	(TOGW) 320,000 lbs. (Fuel) 168,000 lbs. (OEW) 136,000 lbs.
Cruise	M=1.7 L/D = 8.7
Payload	80 pax
Range	> 5000 nm
Boom Strength	(Full carpet) < 85 PLdB
Ground Op	(Wheelbase) 91 ft. 3 in. (Wheeltrack) 14 ft. (Turnover) 60 deg.

was to develop a structural model with a representative global stiffness and mass distribution to enable aeroelastic studies. To facilitate the use of high fidelity CFD based methods, a detailed structural layout was developed, meshed, and structurally optimized to a representative set of load cases consisting of landing, maneuver, and gust loads, subject to strain, buckling, and minimum gauge criteria. A combined image of all of the substructural components of the vehicle is presented in Figure 5.

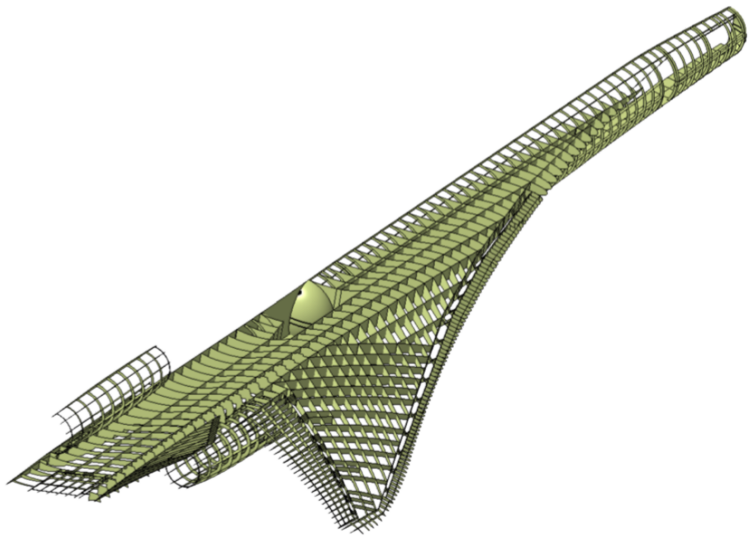

Figure 4: A view of the substructure of the N+2 configuration.

Based on this detailed structural layout, a detailed FEM was developed that captures realistic structural design constraints associated with this class of vehicles. A snapshot of the different sections of the N+2 FEM is presented as Figure 6.

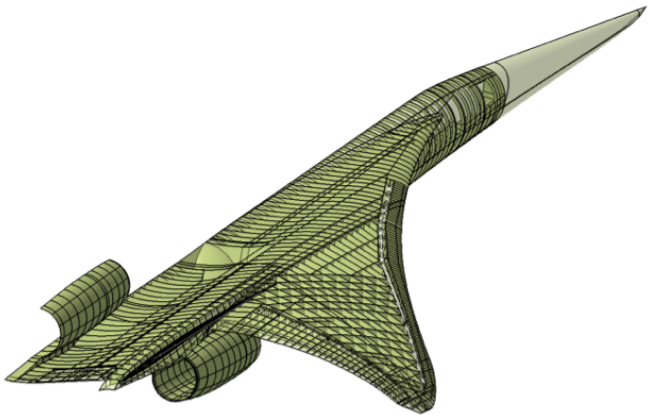

Figure 5: Structural layout of the N+2 configuration.

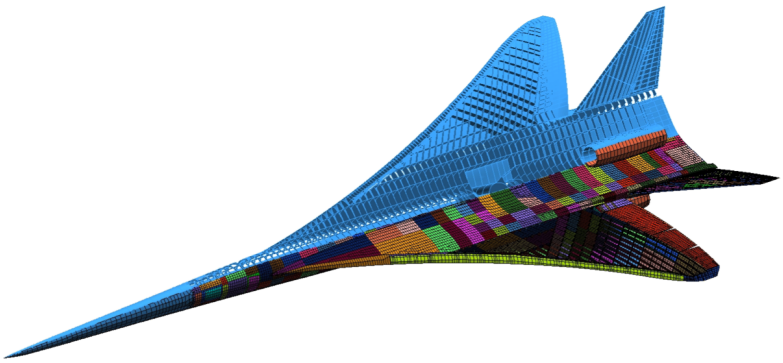

(a) Isometric view.

(b) Aft quarter.

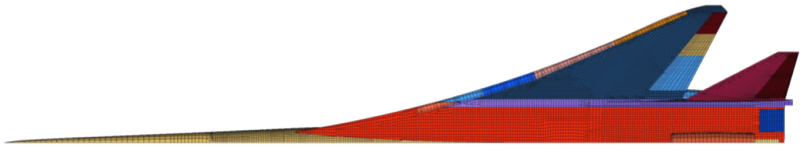

(c) Top view.

Figure 6: Different views of the N+2 FEM.

The finite element model was sized using MSC.Nastran [12] SOL200 assuming the implementation of composite structures. The majority of the FEM was discretized into constant property design zones, and the optimizer was allowed to adjust these properties using the design variables defined within these zones. The skins were assumed to utilize a sandwich approach consisting of Graphite/BMI Unidirectional Tape with a honeycomb core, resulting in three independent design variables per zone (0, ±45, 90 degree plies; core thickness remains constant in sizing). The design of the substructure also assumed

a sandwich approach with Graphite/BMI Fabric facesheets. The approach for the substructure assumed a quasi-isotropic laminate, resulting in one design variable per zone. Core thickness for the substructure also remained constant during sizing. A representative mass distribution was also developed and applied that accounted for systems, payload, and various fuel states. Buckling was included during the optimization by coupling a Lockheed-Martin in-house analysis code along with MSC.Nastran SOL200.

The original all-composite FEM was updated to include metallic materials representative of material utilization on modern aircraft. Figure 7 summarizes the areas where metallics were used. The overall composition percentages for the N+2 were: composites 55%, aluminum 26%, titanium 16%, and steel 3%. The finite element model has roughly 170,000 degrees of freedom.

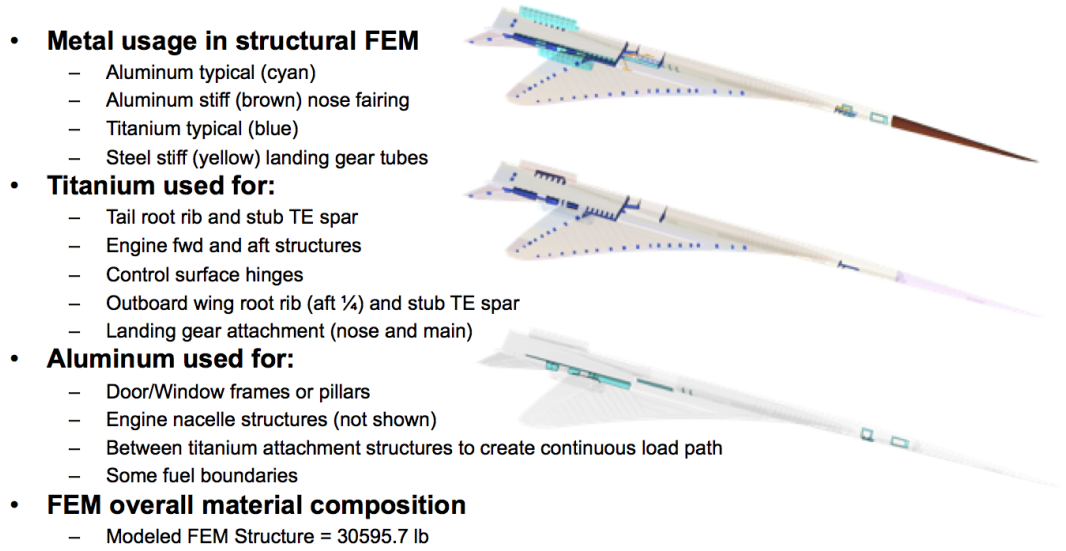

Figure 7: Metallic usage and overall composition of FEM.

In the course of sizing the N+2 vehicle, concerns arose over the tail and aft deck deflections under load. These concerns initiated an effort to modify the FEM to provide better load transfer from the tail to the centerline of the aft fuselage. Details regarding these concerns and the solutions implemented can be found in prior references.

A modal solution was performed on the most recent FEM, the results of which are in the following figures. Not shown are three rigid body modes consistent with symmetric boundary conditions. The first four flexible symmetric modes are presented in Figure 8.

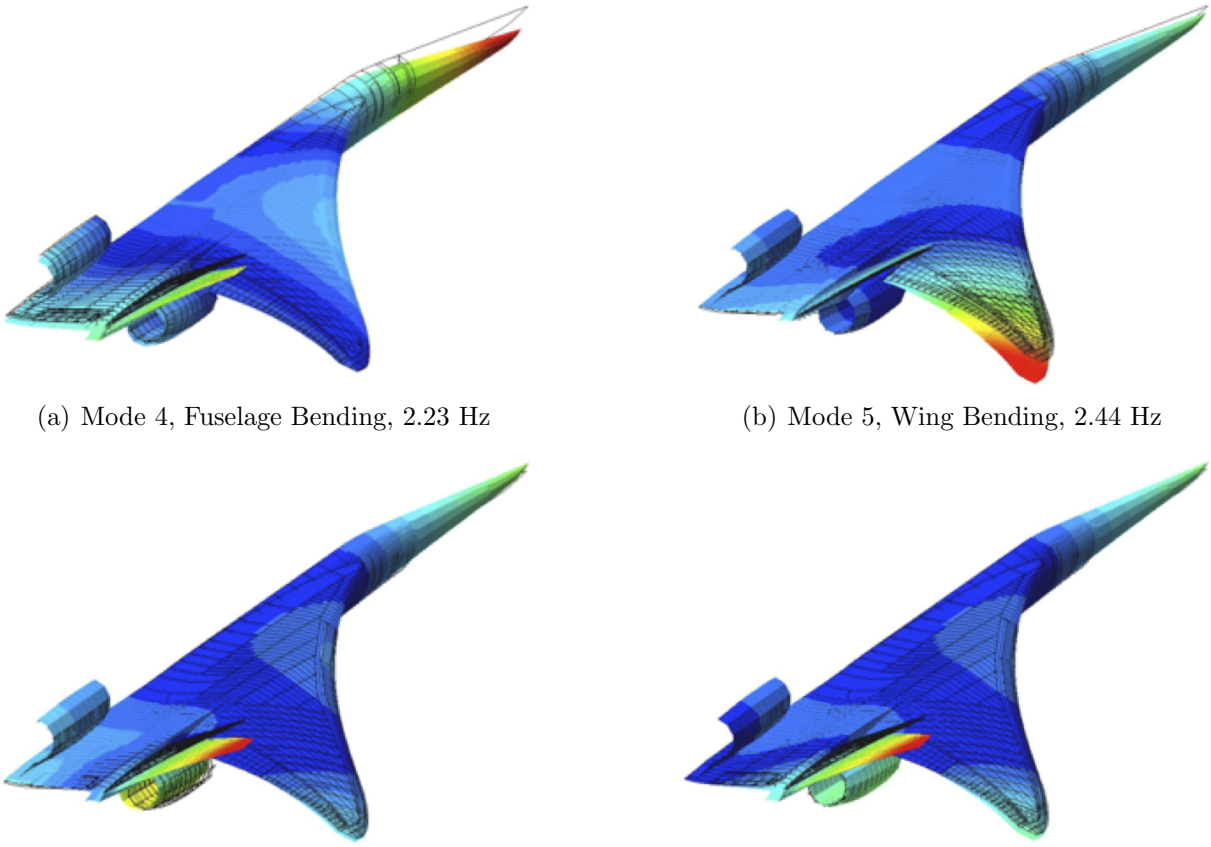

(a) Mode 4, Fuselage Bending, 2.23 Hz

(b) Mode 5, Wing Bending, 2.44 Hz

(c) Mode 6, Tail Bending, 3.38 Hz

(d) Mode 7, Wing Tip Bending-Torsion-Fuselage 2nd Bending, 3.67 Hz

Figure 8: First four symmetric flexible modes, Modes 4-7, for the FEM017-Rev70, full fuel weight condition.

4 LINEAR AEROELASTIC ANALYSES

The N+2 configuration FEM is being used to perform linear and nonlinear AE analyses. This linear AE analyses include the generation of linear subsonic and supersonic frequency-domain unsteady aerodynamics. Presented in Figure 9 is a planform view of the doublet lattice aerodynamic box layout consisting of 1930 boxes.

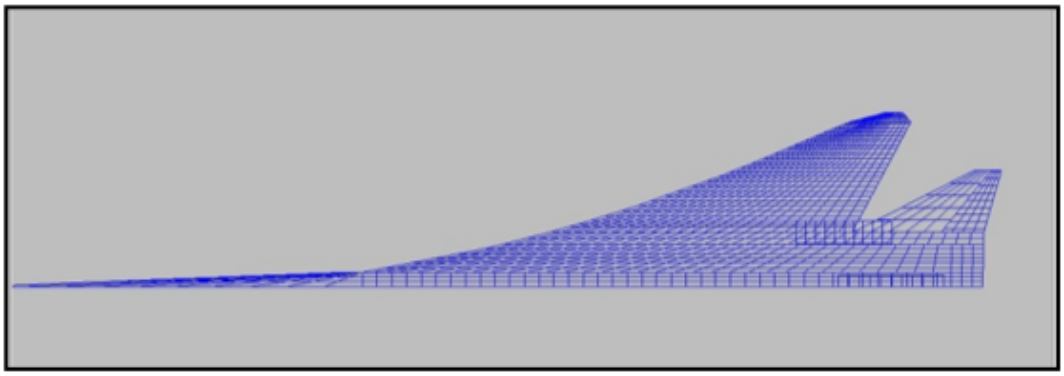

Figure 9: Planform view of the doublet lattice model.

External flight loads were computed via static aeroelastic analysis in MSC.NASTRAN (SOL144). The linear aerodynamic doublet-lattice method available in the solution was used and for initial loads calculations rigid aerodynamics were assumed, eventually transitioning to flexible aerodynamics as the structural design matured. Loads were also developed for a select number of cases using CFD (Euler) predictions.

Figure 10 presents the linear aerodynamic model used both for maneuver loads and flutter analyses. As shown in the figure, there are nine control surfaces, four leading-edge flaps, two ailerons, one trailing-edge flap, one body flap and one rudder. For this semispan aerodynamic model there are 1930 individual aerodynamic boxes. Guidelines for developing the model included: avoiding abrupt element size changes between panels, maintaining streamwise continuity between panels (which required splitting the control surfaces into several pieces), and aiming for boxes with aspect ratios of 1 to 2 as much as possible without letting the number of elements become excessive. Mapping between the aerodynamic model and finite element model is provided via infinite plate splines.

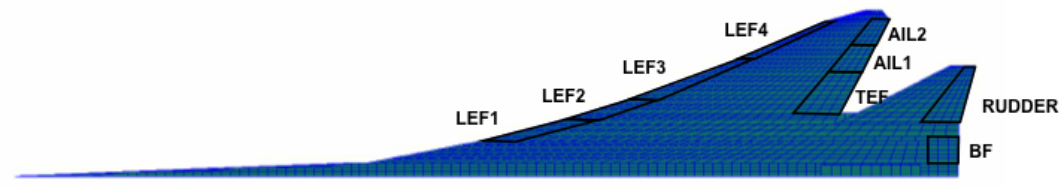

Figure 10: View of the control surface definitions for the doublet lattice model.

Figure 11 is a comparison of the lift curve as predicted by the linear aerodynamic model and compared to supersonic (Mach 1.7) wind tunnel test data. The linear aerodynamic model matches the measured lift curve quite well, especially when fuselage incidence and wing twist are removed from the model. Based on this data and the previous figure,

the incidence and twist were included for subsonic maneuver load cases and removed for supersonic load cases.

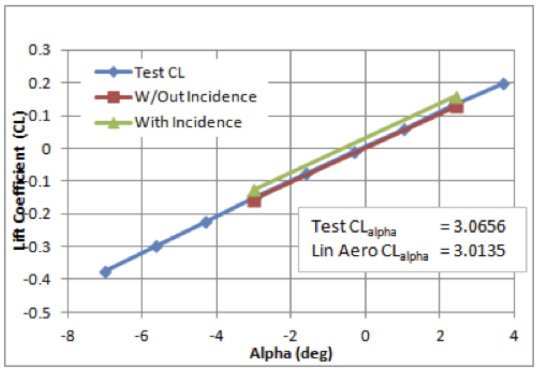

Figure 11: Comparison of linear aerodynamic lift coefficient with test data at Mach = 1.7.

Open-loop flutter analysis was performed on the final structural designs, FEM017-REV70 (sized without the constraint on tail displacement) and FEM017-REV71 (sized with the constraint on tail displacement). The MSC.NASTRAN SOL145 was used to compute flutter solutions, which uses the doublet lattice method for subsonic Mach numbers and the ZONA51 method for supersonic Mach numbers.

Flutter analysis was initially performed on the REV71 structural design, the design that included a displacement constraint on tail deformation. However, for both symmetric and anti-symmetric boundary conditions and for three gross weights, there were no unstable flutter roots below 1600 psf and in most cases, especially for anti-symmetric boundary conditions, there were none below 3500 psf (minimum required flutter dynamic pressure is roughly 900 psf for most Mach numbers). This stood in stark contrast to previous flutter analyses on the all-composite FEM, where critical flutter dynamic pressures around 1000 psf were noticed. As a result, it was speculated that inclusion of the displacement constraint considerably stiffened the tail and aft deck thereby increasing the flutter speed dramatically, which was characterized largely by tail and aft deck bending. Consequently, in order to evaluate a more critical configuration, flutter surveys were performed on the REV70 design, which did not include the tail displacement constraints. The results of these surveys are presented below, indicating flutter speeds that were much lower and closer to the flutter boundary.

Figure 12 shows the minimum flutter dynamic pressure as a function of Mach number and vehicle gross weight for symmetric boundary conditions. In addition, the minimum required flutter dynamic pressure (including the 15% margin on flutter speed) is represented by the solid red line. Flutter dynamic pressure below this line would indicate that the vehicle flutter requirement is not met, and so, based on this linear flutter analysis, we conclude that flutter speed is not critical. The dashed lines indicate that a flutter root was not found within the dynamic pressure range of the analysis (up to about roughly 4000 psf). However, in the transonic region, a more appropriate non-linear transonic flutter solver is needed. For the DTOW (Design Take-Off Weight) and DTOW2 (Design Take-Off Weight 2) flutter solutions, the flutter modes in the 3000-4000 psf range have a

flutter frequency of about 10-12 Hz. The flutter modes that go unstable at lower dynamic pressure near 15002000 psf have flutter frequencies of about 5-6 Hz. The flutter frequency for the ZFW (Zero Fuel Weight) cases ranges from 6-7 Hz.

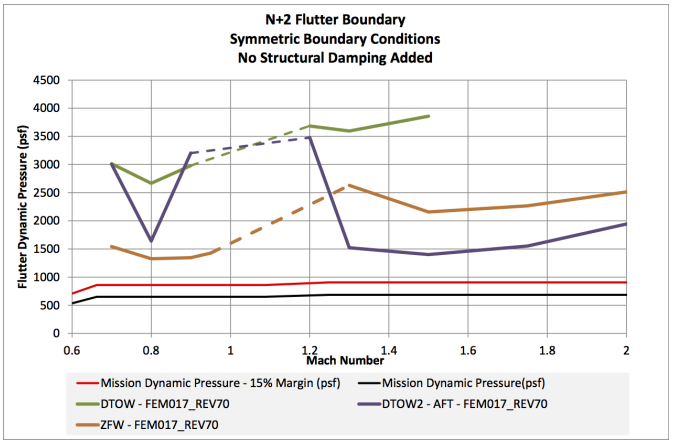

Figure 12: Flutter boundaries based on symmetric mode shapes and linear unsteady aerodynamics for different payload cases.

Figure 13 shows the minimum flutter dynamic pressure as a function of Mach number and vehicle gross weight for anti-symmetric boundary conditions. In general, the flutter speeds are higher than in the symmetric cases.

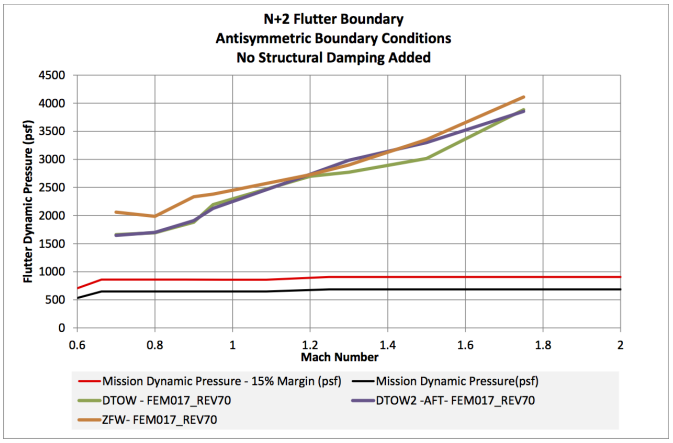

Figure 13: Flutter boundaries based on anti-symmetric mode shapes and linear unsteady aerodynamics for different payload cases.

It can be seen that the most recent version of the REV71 FEM yields improved flutter boundaries across the Mach number range. It should be kept in mind that flutter dynamic pressures predicted by linear aerodynamics are less reliable in the transonic regime and are generally non-conservative. Exactly which Mach numbers define the transonic regime for this configuration is still to be determined. For these reasons, the use of CFD-based aeroelastic analyses becomes a critical part of this research.

5 UNSTRUCTURED GRIDS

Unstructured grids of the N+2 configuration are also being generated for use with the FUN3D code [13]. Multiple grids are being generated to address the configuration with and without engines as well as for inviscid and viscous analyses. Within the code, the unsteady Navier-Stokes equations are discretized over the median dual volume surrounding each mesh point, balancing the time rate of change of the averaged conserved variables in each dual volume with the flux of mass, momentum and energy through the instantaneous surface of the control volume. Additional details regarding the aeroelastic capability within the FUN3D code can be found in the references [14].

Presented in Figure 14 is a forward view of the inviscid unstructured surface grid recently generated. Figure 15 presents a zoomed-in front view of the flow-through nacelles. The half-plane unstructured surface grid has 298,085 points and 555,710 cells.

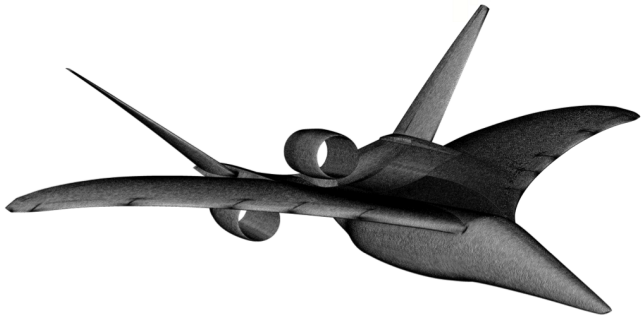

Figure 14: Forward view of the inviscid unstructured grid.

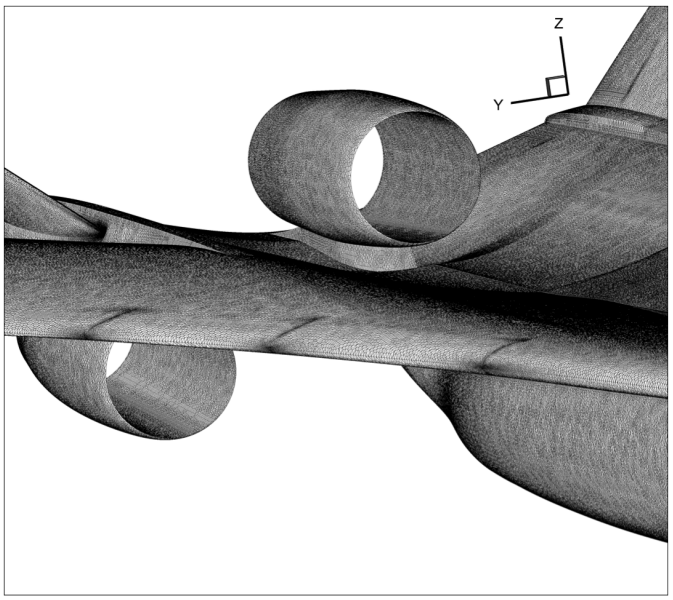

Figure 15: Zoomed-in view of the flow-through nacelles in the inviscid unstructured surface grid.

Grids that were generated initially were used for preliminary static aeroelastic analyses. However, these grids had to be modified and adapted in order to perform accurate sonic boom analyses. Therefore, the coarse grid used for the static aeroelastic analysis is not the same coarse grid that was used for the sonic boom analysis.

Presented in Figure 16 is a steady inviscid (Euler) FUN3D solution at cruise condition using a coarse grid. Presented in Figure 17 is a steady inviscid (Euler) FUN3D solution at cruise condition using a fine grid. Preliminary comparison of performance parameters between the two grids indicates very minor differences thereby permitting the use of the coarse grid for most analyses. Figure 18 presents a static aeroelastic computation for the FUN3D Euler (inviscid) coarse grid at cruise condition using the first 25 flexible modes. Results indicate a static aeroelastic deformation of about six inches at the wing tip and tail.

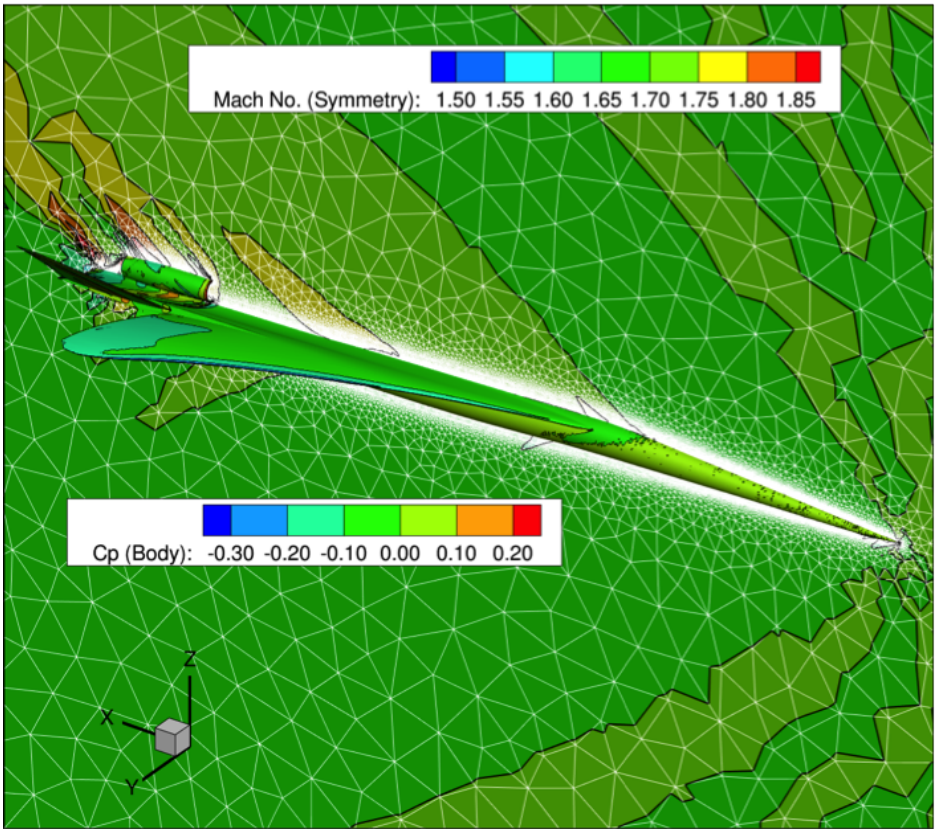

Figure 16: Coarse grid (5.4 million) FUN3D steady (undeformed) Euler (inviscid) result at cruise condition.

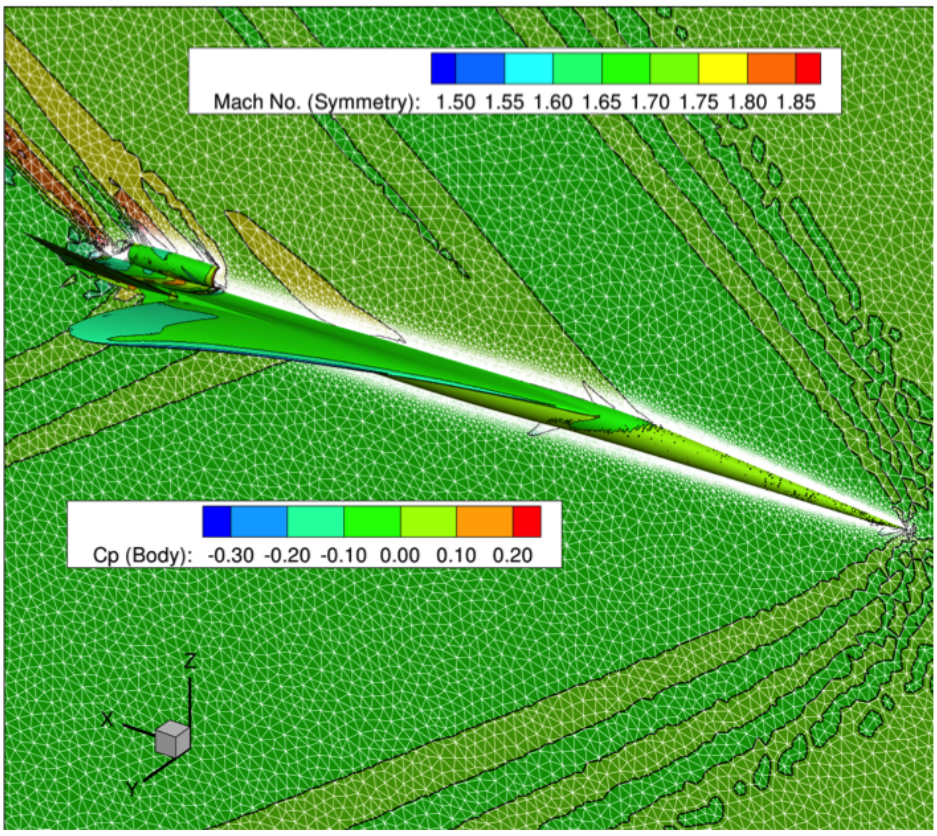

Figure 17: Fine grid (57.5 million) FUN3D steady (undeformed) Euler (inviscid) result at cruise condition.

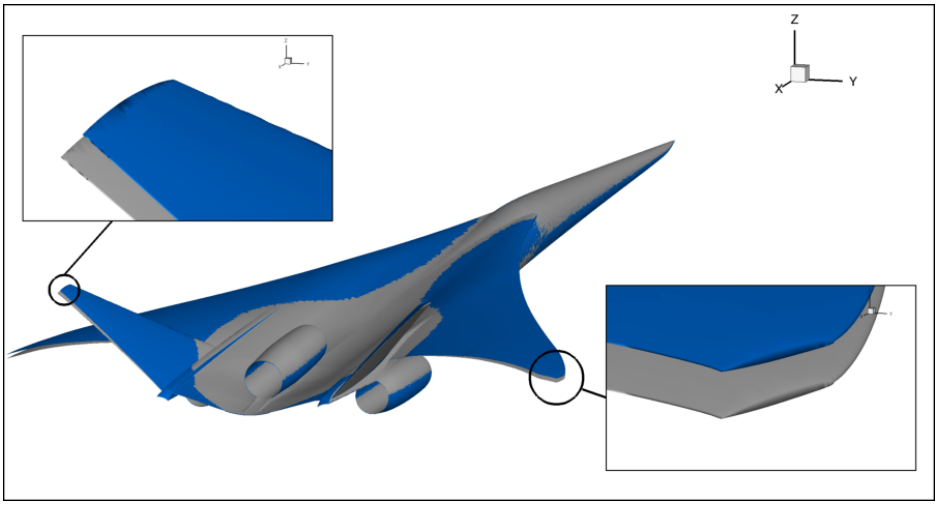

Figure 18: Coarse grid FUN3D static aeroelastic Euler (inviscid) deformation at cruise condition. Blue surface is deformed shape.

In order to compute the effect of this static aeroelastic deformation on sonic boom, a near-field region is defined that is 8.25 half-spans away from the configuration at the cruise condition, presented in Figure 19.

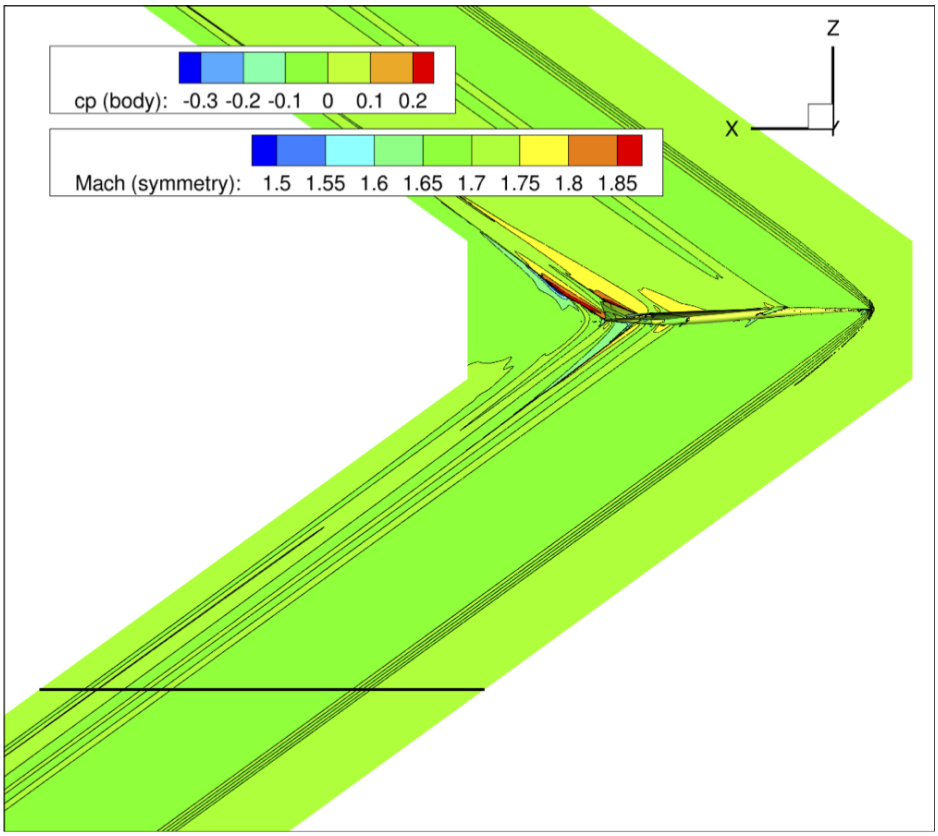

Figure 19: Coarse grid FUN3D steady (undeformed) Euler (inviscid) near field definition at 8.25 half-spans away at cruise condition.

A comparison of near-field pressure results at the prescribed near-field location for different grid densities (coarse, medium, and fine) is presented as Figure 20. There appear to be some slight differences for the coarse grid solution while the medium and fine grid solutions appear to be more closely correlated. Although the coarse grid is being used for these preliminary sonic boom assessments, solutions using the medium and fine density grids are currently underway.

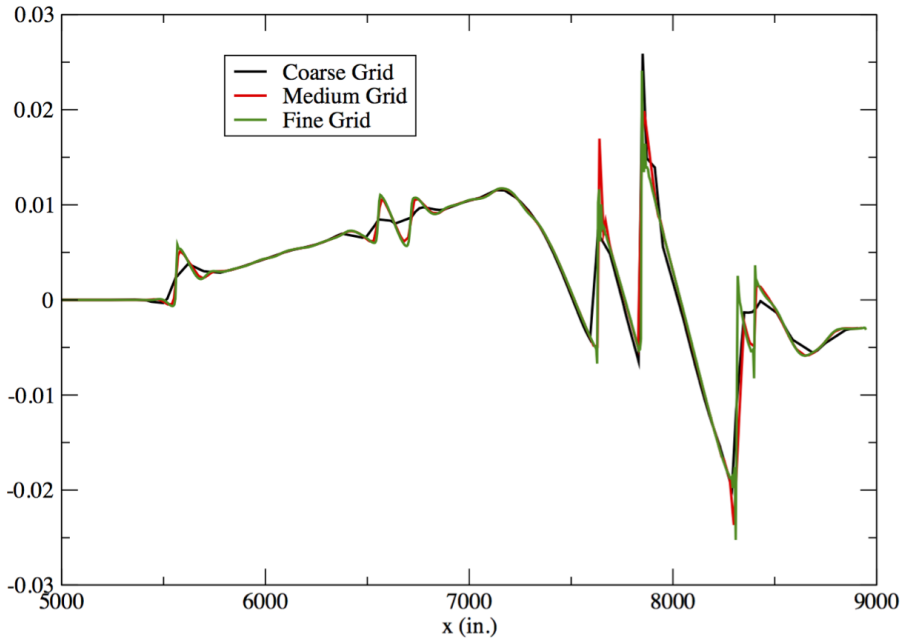

Figure 20: Near-field pressure distribution for the undeformed case for different grid densities.

Presented in Figure 21 is a comparison of the near-field pressure distributions for the undeformed and deformed conditions. As can be seen in the figure, the static aeroelastic deformation tends to unload the vehicle, thus resulting in the modified pressure distribution, particularly in the region of the wing.

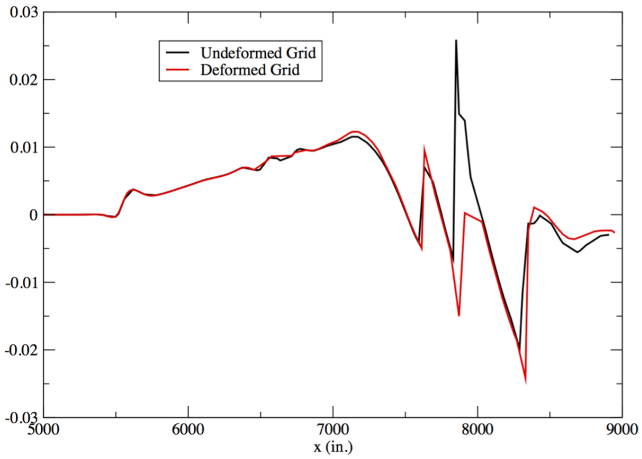

Figure 21: Near-field pressure distribution for the undeformed and deformed configurations.

Recent work has focused on the creation of improved grids that are better suited for sonic boom propagation. Given that the grids generally used for aeroelastic analyses are not well suited for sonic boom propagation, several parametric studies have been performed

in order to develop the best possible grids for both aeroelastic analyses and sonic boom propagation. Presented in Figure 22 is a close-up detail of the grid used for standard computational aeroelastic analyses.

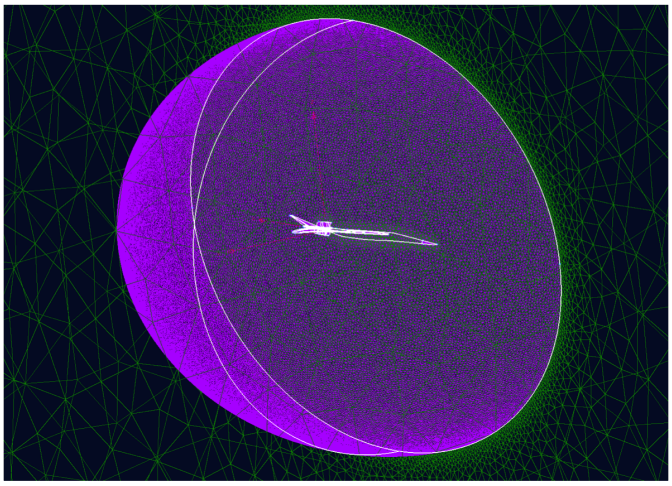

Figure 22: Close-up detail of the grid used for aeroelastic analyses.

Presented in Figure 23 is a close-up detail of one of the grids used for sonic boom propagation. Multiple grids were generated for sonic boom propagation studies with grid dimensions of 16 million grid points (coarse), 45 million grid points (medium), and 90 million grid points (fine).

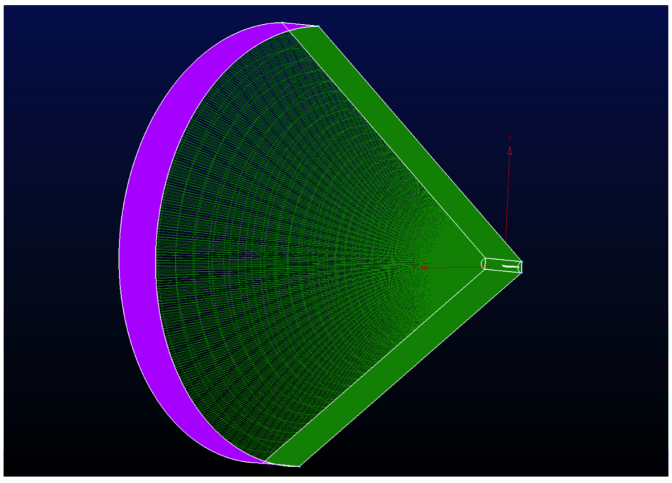

Figure 23: Close-up detail of one of the grids used for sonic boom propagation analyses.

Presented in Figure 24 is a close-up view of a sonic boom analysis using the coarse grid indicating a decent capture of the bow shock. Presented in Figure 25 is a comparison of the ground level boom signature for the three different grids for the configuration with no engines at Mach = 1.7 and alpha = 2.25 degrees. As can be seen, use of the finer grid exhibits some variation near the middle of the signature not seen with the coarse and

medium density grids.

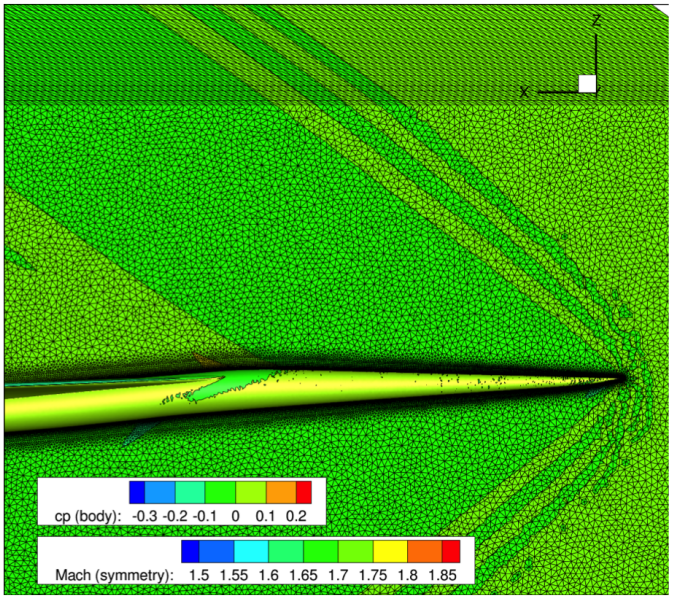

Figure 24: Close-up detail of the bow shock for sonic boom analyses using the coarse grid.

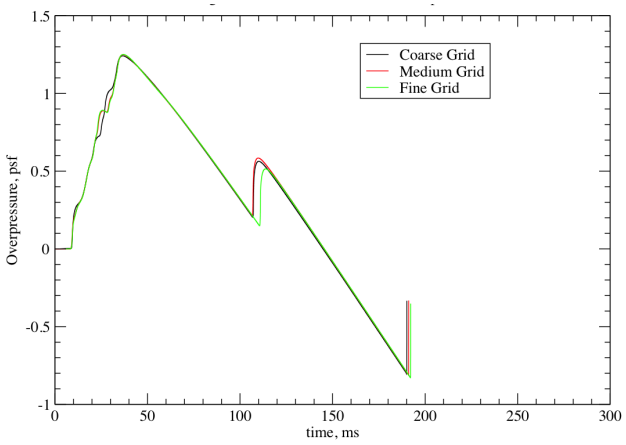

Figure 25: Ground-level boom signature at cruise for various grid densities.

Presented in Figure 26 is a comparison of the ground level boom signature for the undeformed and deformed conditions for the configuration with no engines at Mach = 1.7 and alpha = 2.25 degrees. There is clearly an effect of the static aeroelastic deflection on the ground-level boom signature. However, additional analyses are required to better understand the implications of this result.

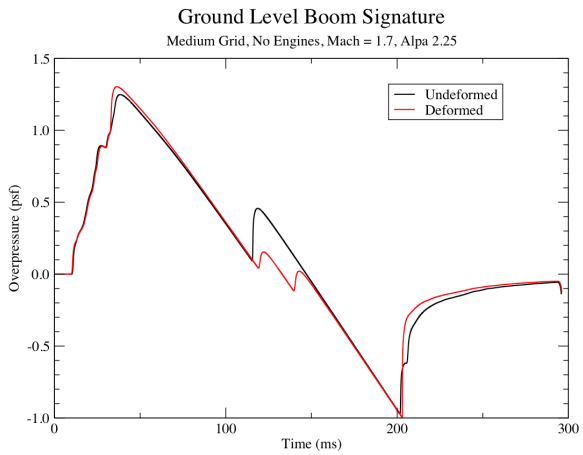

Figure 26: Ground-level boom signature at cruise for the undeformed and deformed cases.

6 REDUCED ORDER MODELS

The goal behind the development of a ROM for the rapid computation of unsteady aerodynamic and aeroelastic responses is aimed at addressing two challenges. The first challenge is the computational cost associated with full CFD aeroelastic simulations, which increases with the fidelity of the nonlinear aerodynamic equations to be solved as well as the complexity of the configuration. Computational cost, however, may be reduced via the implementation of parallel processing techniques, advanced algorithms, and improved computer hardware processing speeds.

The second, more serious, challenge is that the information generated by these simulations cannot be used effectively within a preliminary design environment. Because the output of these full CFD aeroelastic simulations cannot be incorporated within a design environment, parametric variations and design studies can only be performed by trial-and-error. As a result, the integration of computational aeroelastic simulations into preliminary design activities involving disciplines such as aeroelasticity, ASE, and optimization continues to be a costly and impractical venture.

However, with the development of ROM methods [15–17], the rapid generation of root locus plots using CFD-based unsteady aerodynamics is now available to aeroelasticians. This recently developed technology is being applied to the N+2 supersonic configuration for evaluation of aeroelastic mechanisms across several Mach numbers. A sample of some of those results is presented in the following.

An aeroelastic ROM has been developed at the cruise Mach number of 1.7. Presented in Figure 27 is a comparison of the dynamic aeroelastic response from a full FUN3D aeroelastic solution and the ROM aeroelastic solution at a dynamic pressure of 2.149 psi where the time histories of the fourth mode generalized displacements are compared. As can be seen, the results are practically identical. Similar results are obtained for all the other modes, indicating good confidence in the ROM.

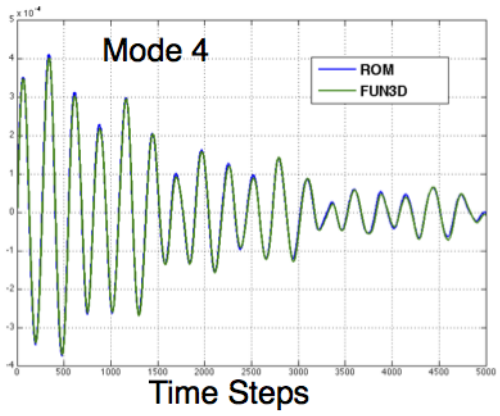

Figure 27: Comparison of full FUN3D aeroelastic response and ROM aeroelastic response for the fourth mode at M=1.7 and a dynamic pressure of 2.149 psi.

A major benefit of this ROM technology is the ability to rapidly generate an aeroelastic root locus plot that reveals the aeroelastic mechanisms occurring at that flight condition. Presented in Figure 28 is the aeroelastic root locus plot with a variation in dynamic pressure. As can be seen, the flutter mechanism is related to a coalescence of the fifth and sixth modes. There also appears to be an interesting blending of the second and fourth modes.

In the root locus plot, each symbol represents the aeroelastic roots at a specific dynamic pressure. In this case, each increment in dynamic pressure corresponds to 1 psi. It is important to mention that this root locus plot is generated in seconds while multiple full FUN3D solutions would be required for each dynamic pressure of interest.

The computational cost of generating these ROM solutions consists of one full FUN3D solution that is used to generate the ROM at that Mach number. This full FUN3D solution ran for three hours and consisted of 2400 time steps. Once this solution is available, a ROM can be generated and then used to generate all the aeroelastic responses at all dynamic pressures. In comparison, a full FUN3D analysis at each dynamic pressure requires two full FUN3D solutions: a static aeroelastic (10 hours) and a dynamic aeroelastic (18 hours). Therefore, full FUN3D solutions for 20 dynamic pressures would require 560 hours of compute time.

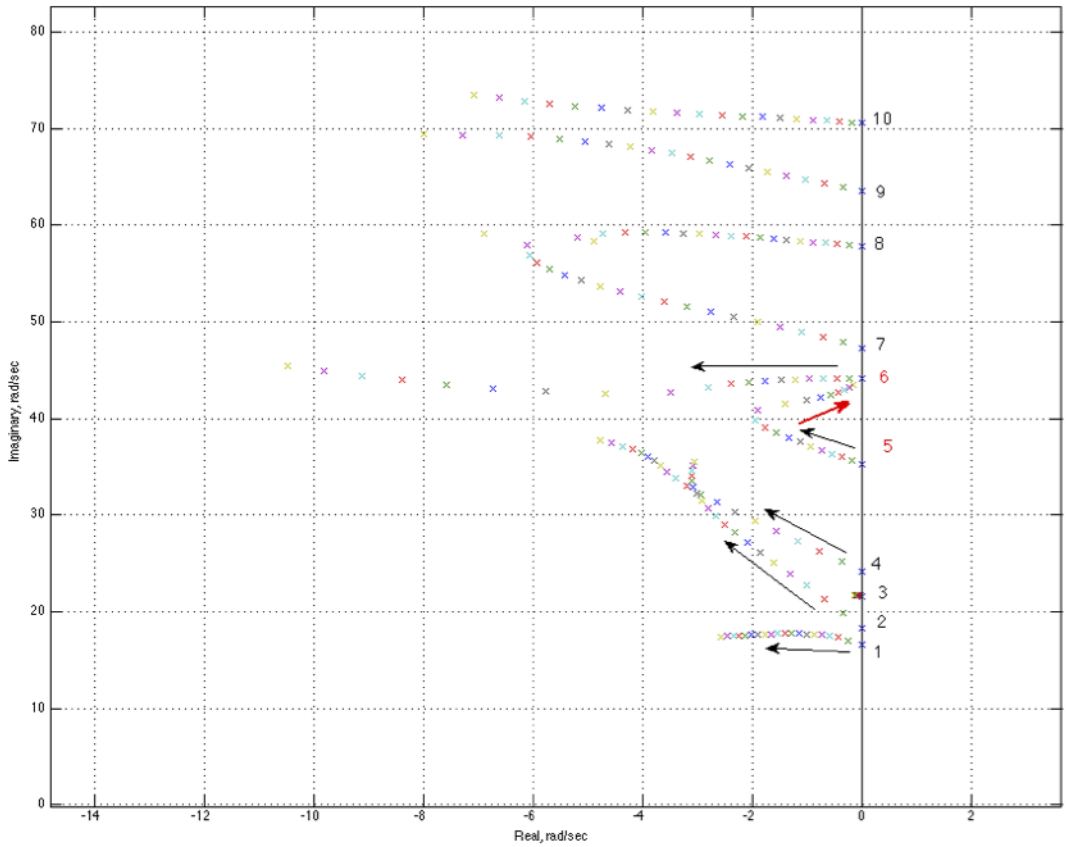

Figure 28: Aeroelastic root locus plot for the cruise condition at M=1.7 with each colored marker indicating a different dynamic pressure for a given mode.

7 AERO-PROPULSO-SERVO-ELASTICITY

To conduct the APSE studies, the propulsion system model needs to be integrated into a CFD solver that is capable of modeling aero-elastic effects of a commercial supersonic vehicle, such as FUN3D. Up until now, FUN3D could simulate inlet and nozzle flows, but not the effect of any turbo machinery components that may influence those flows. Air breathing propulsion simulation in FUN3D is currently constrained to independently specify outflow conditions at an engine inlet face, typically static pressure ratio; and inflow conditions into a nozzle geometry, typically total pressure and total temperature in the case of modeling the upstream subsonic plenum, or supersonic inflow in the case of modeling the nozzle downstream of the throat. Current efforts have allowed for a previously developed Variable Cycle Engine (VCE) that will provide a new capability by creating a C code library of the engine model that can be read by FUN3D at simulation startup. The current proof-of-concept configuration is a fully 3D engine nacelle with an external compression axi-symmetric inlet and a three-flow path convergent-divergent nozzle. These two complicated component models are connected by the quasi 1D C-library VCE model. The engine model uses the average total pressure and temperature from the

solution at the inlet face coming from the 3D flow solver and calculates the nozzle inflow boundary conditions.

Previously, propulsion systems in FUN3D just modeled the place in the simulation for the gas turbine engine as a hollow tube. This new feature now allows for the accurate propagation of the flow condition at the inlet-engine boundary to the engine-nozzle boundary. A preliminary result of the steady-state Mach number contours is shown in Fig. 29. This preliminary result illustrates the Mach 1.7, 50,000ft, and 100% power condition and exhibits the expected main features of the flow field with a normal shock near the inlet cowl and the nozzle flow capturing the complex interactions of the various speed of the flow exiting the three nozzles. On-going work is needed to gain certainty of the results, however, the main goal of interfacing the two simulation environments was achieved. Additional work is currently underway to investigate the unsteady behavior of the simulation before using this new capability in APSE studies.

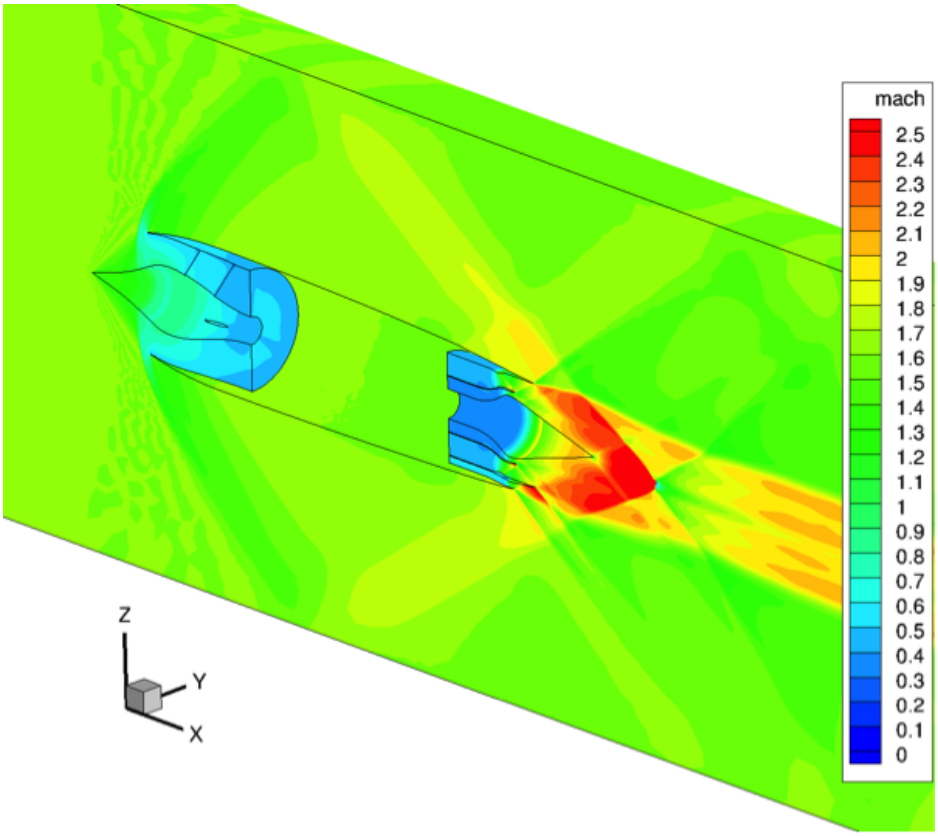

Figure 29: FUN3D propulsion system model with VCE lumped volume model steady-state Mach profile.

8 CONCLUDING REMARKS

A summary of recent developments performed by NASA's CST-ASE element was presented. The summary included a discussion of the low-boom N+2 configuration and related FEM developed by Lockheed-Martin. Results presented include linear flutter boundaries based on updated and improved versions of the original FEM. Unstructured CFD grids (inviscid, viscous, with/without engines) were generated and used with the FUN3D CFD code. Steady rigid and static aeroelastic results at a cruise condition were

computed including the effects of static aeroelastic deformation on the near-field and the ground-level sonic boom signature. Finally, brief overviews of the ongoing work related to the application of the ROM methodology and the APSE model development were provided.

9 REFERENCES

[1] (1995). Advanced aeroservoelastic testing and data analysis. In *AGARD Conference Proceedings 566, NATO*.

[2] Noll, T. E. (1990). Aeroservoelasticity. In *31st AIAA/ASME/ASCE/AHS/ASC Structures, Structural Dynamics and Materials Conference*, 1990-29359. Long Beach, CA.

[3] Sandford, M. C., Abel, I., and Gray, D. L. (1975). Development and demonstration of a flutter-suppression system using active controls. In *NASA TR R-450*.

[4] Abel, I., Perry, B., and Newsom, J. R. (1982). Comparison of analytical and wind-tunnel results for flutter and gust response of a transport wing with active controls. In *NASA TP 2010*.

[5] Waszak, M. R. (1997). Robust multivariable flutter suppression for the benchmark active control technology (bact) wind-tunnel model. In *Eleventh Symposium on Structural Dynamics and Control*.

[6] Perry, B., Cole, S. R., and Miller, G. D. (1995). Summary of an active flexible wing program. In *Journal of Aircraft*, vol. 32. pp. 10–15.

[7] Pendleton, E. W., Bessette, D., Field, P. B., et al. (2000). Active aeroelastic wing flight research program technical program and model analytical development. In *Journal of Aircraft*, vol. 37.

[8] Silva, W. A., Keller, D. F., Florance, J. R., et al. (2000). Experimental steady and unsteady aerodynamic and flutter results for hsct semispan models. In *AIAA/ASME/ASCE/AHS/ASC 41st Structures, Structural Dynamics, and Materials Conference*, 2000-1697.

[9] Perry, B., Silva, W. A., Florance, J. R., et al. (2007). Plans and status of wind-tunnel testing employing an aeroservoelastic semispan model. In *48th AIAA/ASME/ASCE/AHS/ASC Structures, Structural Dynamics, and Materials Conference*, AIAA Paper No. 2007-1770. Honolulu, HI.

[10] Silva, W. A., Garza, A. D. L., Zink, P. S., et al. (2014). The nasa high speed ase project: Computational analyses of a low-boom supersonic configuration. In *55th AIAA/ASMe/ASCE/AHS/SC Structures, Structural Dynamics, and Materials Conference*, 2014-0675.

[11] Silva, W. A., Garza, A. D. L., Zink, P. S., et al. (2015). An overview of the nasa high speed ase project: Aeroelastic analyses of a low-boom supersonic configuration. In *56th AIAA/ASCE/AHS/SC Structures, Structural Dynamics, and Materials Conference*, 2015-0684.

[12] http://www.mscsoftware.com/product/msc nastran.

[13] Anderson, W. K. and Bonhaus, D. L. (1994). An implicit upwind algorithm for computing turbulent flows on unstructured grids. *Computers and Fluids*, 23(1), 1–21.

[14] Biedron, R. T. and Thomas, J. L. (January 2009). Recent enhancements to the fun3d flow solver for moving mesh applications. In *47th AIAA Aerospace Sciences Meeting, Orlando, FL*.

[15] Silva, W. A. (July-August 2008). Simultaneous excitation of multiple-input/multiple-output cfd-based unsteady aerodynamic systems. *Journal of Aircraft*, 45(4), 1267–1274.

[16] Silva, W. A., Vatsa, V. N., and Biedron, R. T. Development of unsteady aerodynamic and aeroelastic reduced-order models using the fun3d code. IFASD Paper No. 2009-30, presented at the International Forum on Aeroelasticity and Structural Dynamics, Seattle, WA.

[17] Silva, W. A., Vatsa, V. N., and Biedron, R. T. Reduced-order models for the aeroelastic analyses of the ares vehicles. AIAA Paper No. 2010-4375, presented at the 28th AIAA Applied Aerodynamics Conference, Chicago, IL.